View metadata, citation and similar papers at core.ac.uk

brought to you by CORE

provided by HKU Scholars Hub

The HKU Scholars Hub The University of Hong Kong 香港大學學術庫

Title	Post Asymptotic Giant Branch Bipolar Reflection Nebulae: Result of Dynamical Ejection or Selective Illumination?
Author(s)	Koning, N; Kwok, S; Steffen, W
Citation	The Astrophysical Journal, 2013, v. 765, p. 92
Issued Date	2013
URL	http://hdl.handle.net/10722/181841
Rights	Creative Commons: Attribution 3.0 Hong Kong License

The Astrophysical Journal, 765:92 (8pp), 2013 March 10 doi:10.1088/0004-637X/765/2/92
© 2013. The American Astronomical Society. All rights reserved. Printed in the U.S.A.

POST ASYMPTOTIC GIANT BRANCH BIPOLAR REFLECTION NEBULAE: RESULT OF DYNAMICAL EJECTION OR SELECTIVE ILLUMINATION?

N. Koning[1], Sun Kwok (郭新)[2], and W. Steffen[3]
[1] Department of Physics & Astronomy, University of Calgary, Calgary, Alberta T2N 1N4, Canada; nico.koning@ucalgary.ca
[2] Department of Physics, The University of Hong Kong, Pokfulam, Hong Kong, China; sunkwok@hku.hk
[3] Intituto de Astronomía Universidad Nacional Autónoma de México, C.P. 22860, Ensenada, Mexico; wsteffen@astrosen.unam.mx
Received 2012 June 19; accepted 2013 January 17; published 2013 February 20

ABSTRACT

A model for post asymptotic giant branch bipolar reflection nebulae has been constructed based on a pair of evacuated cavities in a spherical dust envelope. Many of the observed features of bipolar nebulae, including filled bipolar lobes, an equatorial torus, searchlight beams, and a bright central light source, can be reproduced. The effects on orientation and dust densities are studied and comparisons with some observed examples are offered. We suggest that many observed properties of bipolar nebulae are the result of optical effects and any physical modeling of these nebulae has to take these factors into consideration.

Key words: planetary nebulae: general – stars: AGB and post-AGB – circumstellar matter

Online-only material: color figures

1. INTRODUCTION

Objects in transition between the asymptotic giant branch (AGB) stars and planetary nebulae (PNs) constitute a subclass of reflection nebulae. In this intermediate evolutionary stage, the temperature of the central star is too low to photoionize the circumstellar envelope, and the optical brightness of these transition objects (commonly called "proto-planetary nebulae," or PPNs) are entirely due to scattered light. Since AGB stars are spherical, the emergence of bipolar shapes in PPNs and PNs raises questions on what physical mechanisms are responsible for this morphological transformation. The most well-known bipolar post-AGB object is AFGL 2688 (the Egg Nebula, Sahai et al. 1998). Other examples include He 3−401 (García-Lario et al. 1999), IRAS 10197−5750 (Roberts 22, Hrivnak et al. 2008), M 1−92 (Bujarrabal et al. 1998), IRAS 17150−3224 (the Cotton Candy Nebula, Kwok et al. 1998), IRAS 17106−3046 (Kwok et al. 2000), and IRAS 12419−5414 (the Boomerang Nebula, Sahai & Nyman 1997). These nebulae show a pair of optical lobes centered on a low-temperature (<20,000 K) star. The temperature of the central stars within these nebulae are too low to produce emission lines and the colors of the lobes suggest that their brightness originates from dust scattering of light from the central star. Most of these objects also show strong infrared excesses due to thermal emission by dust. Observational properties of PPN are summarized by Kwok (1993).

The commonly held assumption is that the bipolar lobes themselves represent dense mass ejection events, and binary stars (e.g., De Marco et al. 2004) or magnetic fields (e.g., García-Segura et al. 1999) have been suggested as the means of ejection (see Balick & Frank 2002 for a review of possible shaping mechanisms). However, the optical lobes often show sharp boundaries, which suggest that the lobes are confined by an external medium. The strong infrared excesses observed in these objects also suggest that there is a significant amount of dust in the system. It is likely that the observed optical nebulae only represents a small fraction of their total mass, with the majority of mass residing outside the visible lobes. Direct detection of this dust component can be done by ground- and space-based mid-infrared observations (Su et al. 2004; Muthumariappan et al. 2006; Lagadec et al. 2011).

It has been argued that the bipolar lobes represent cavities bounded by this extensive circumstellar dust component and that the light we see from PPNs may in fact represent regions mostly devoid of matter (Kwok 2004, 2010). Evidence for this has been observed in M1−92 (Bujarrabal et al. 1998; Alcolea et al. 2007) and CRL 618 (Sánchez-Contreras et al. 2002; Bujarrabal et al. 2010). Since we see these objects through scattered light, it is possible that light is reflected off the inner walls of the cavity, thereby giving the false impression of a volume filled structure. If true, then the visible apparent morphology of PPNs may differ greatly from the density distribution of matter in these objects. In this paper, we report some computer simulation exercises to test this hypothesis.

2. THE MODEL

The models used in our simulations were generated using the morpho-kinematic software SHAPE (Steffen et al. 2011). The structures have been modeled with static volume meshes to which dust properties have been assigned. The radiation transport is computed on a regular Cartesian three-dimensional grid. In order to speed up numerical computation, cells that are not within the volume meshes are flagged and not used in the radiation transfer.

The radiation transport is performed in two steps. In the first step, for each grid cell the radiation is transferred along a conical ray going from the central source to the cell. The opening angle of the conical ray is determined by the solid angle that the cell has as seen from the central source. The arriving energy is computed as well as the local scattering probability in the direction to the observer. Each cell is assumed to have constant physical properties throughout its volume. The path length through each cell is computed from the positions of its corners and the direction of the ray. The extinction coefficient through the cell is then computed from the path length and the sum of the mean coefficients for scattering and absorption (κ_λ^{sc}, κ_λ^{ab}) for each wavelength band (λ, $\Delta\lambda$), where λ is the central wavelength of the band and $\Delta\lambda$ is the width of the band. This first step is done independently for each cell that contains dust.

In the second radiation transfer step, for each image pixel, a ray is cast into the pre-computed grid and for each cell that this ray crosses the scattered radiation is transferred to the

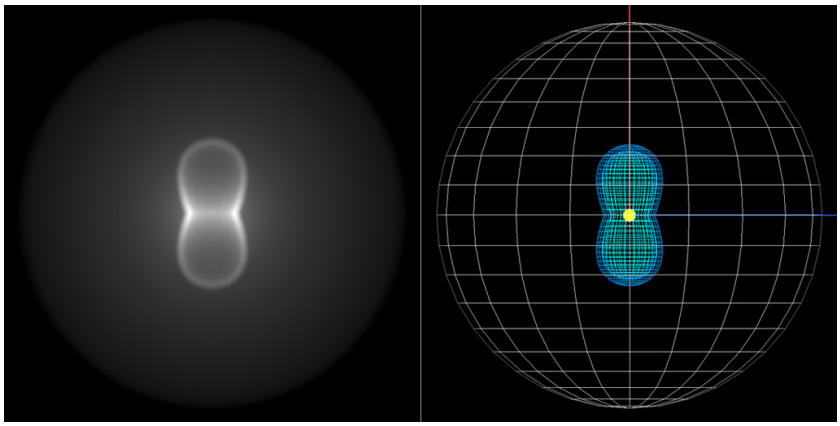

Figure 1. Left: a gray scale presentation of the column density distribution of the model from a view perpendicular to the bipolar axis. The brightness of the image is presented on a square-root scale. Right: a mesh presentation of the model.

(A color version of this figure is available in the online journal.)

image pixel in the same manner as from the radiation source the cell.

The model has three components: (1) a dust halo; (2) a bipolar cavity; and (3) an illuminating central star. The basic premise of this model is that light from the central star is scattered from the walls of the cavity, which gives rise to the optical image of the nebula. Our proposal is that the apparently complicated morphologies of the observed nebular images are the result of absorption and scattering of the central star light by circumstellar dust. The dust density distribution and the three-dimensional mesh geometry of this model is shown in Figure 1. The parameters of the three components along with those used for the renderings are presented in the following sections.

2.1. Dust Halo

The dust halo is spherical in geometry with a radius of $3''$ (this value is large enough to demonstrate the illumination effects and still be computationally viable). The density of the dust decreases as $n(r) = Ar^{-2}$ to simulate the geometrical dilution as the dust expands. The size and density profile of the halo is fixed, but the magnitude, A (units of m^{-1}), is a variable parameter in this model.

The grains consist mostly of amorphous carbon (80% by number) with some silicates (10%) and graphite (10%). The amorphous carbon and silicates range in radius from $a = 20$ nm to $a = 240$ nm with an MRN (Mathis et al. 1977) size distribution. The graphite component consists of small spherical grains with a radius ranging from $a = 1$ nm to $a = 10$ nm, also with an $n(a) \propto a^{-3.5}$ MRN size distribution. Isotopic scattering is assumed.

The refractive and absorption index for amorphous carbon is much higher than that for silicates in our modeled frequency range (visible spectrum). Therefore, a higher abundance of carbon implies more absorption, whereas a higher abundance of silicates implies less absorption. Therefore, it is possible to substitute lower overall densities with a higher silicate composition in the simulations below (to a point).

2.2. Bipolar Cavity

We choose a bipolar shape for our cavity because bipolar (and multipolar) morphologies are frequently observed in both PNs and PPNs (Sahai et al. 2007). Investigating illumination effects in alternative cavity shapes will be left for future work.

The cavity is a region of lower or no density within the dust halo. The cavity is geometrically represented as a sphere with a pinched waist. The cavity has a thin, high density shell that simulates the swept up dust. The thickness of the shell is constant at $0''.1$ and has a density of $n_s = 10n_0$, where n_0 is the density of the ambient halo dust. Although the general bipolar shape of the cavity is maintained in our model, the vertical extent of the cavity is varied (simulating an expanding cavity).

2.3. Central Star

The central star parameters are fixed and do not vary throughout the simulations. The temperature is cool enough such that ionization will not occur and is set to 8800 K. The luminosity of the central star is arbitrarily set to $10^4\ L_\odot$, giving a central star radius of 3×10^{10} m. For the purpose of this study, the most relevant parameter is the temperature, and the assumed luminosity (and stellar radius) has no significant effect of the results.

2.4. Render Parameters

The simulations are computed on a 256^3 grid using single scattering. The spectral distribution of light consists of 10 spectral bands ranging over wavelengths from 400 to 700 nm in equal wavelength intervals, representing the visible portion of the spectrum. For visualization purposes, each wavelength is assigned its visible color. The brightness scale of the images is linear unless otherwise noted and a convolution with a Gaussian kernel of $0''.05$ is applied in order to mask any aliasing effects introduced by the rendering of a regular three-dimensional mesh onto a regular pixel image. The rendered images are 512×512 in pixel size, corresponding to $3'' \times 3''$ in angular extent. The distance to our model nebula is set at 1 kpc.

3. RESULTS

Varying any of the parameters of the aforementioned model can have drastic effects on the observed morphology of the model. This section investigates the effects each parameter independently has on the observed morphology. There is no doubt that individual bipolar nebulae vary in most, if not all, of these parameters. The investigation of simultaneously varying multiple parameters to reproduce morphologies seen in actual objects will be deferred to a later paper. The current methodology provides some valuable insights into the true structure of bipolar

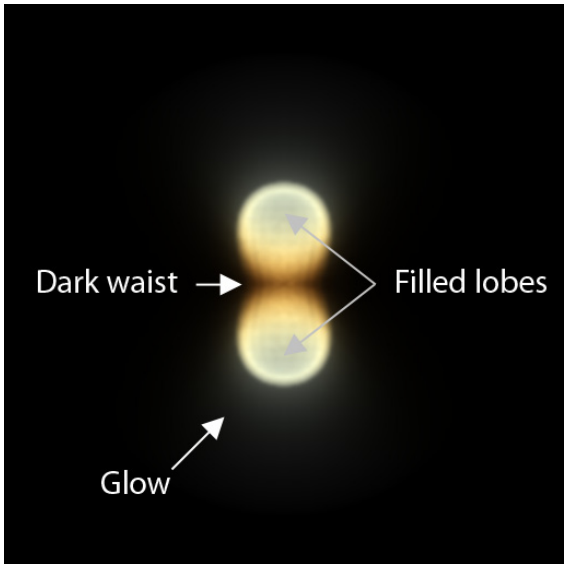

Figure 2. Rendered image of the model. Several features commonly seen in reflection nebulae are evident in this simple model, including a dark waist and the appearance of volume filled lobes.

(A color version of this figure is available in the online journal.)

nebulae and can in fact produce morphologies quite similar to those observed.

3.1. The Basic Model

Figure 2 shows the rendering of the model with the default parameters as given in Section 2. Immediately apparent are several optical effects. First, the light appears to come from within the volume of the bipolar cavity. This is just an illusion.

The solid appearance of the lobes is created by the increase in opacity at small radii. At these larger opacities, the fronts of the lobes are equal in brightness to the edges, thereby creating the solid look. Near the tips of the bipolar lobes, the density, and therefore optical thickness, is less and we begin to see a hint of the shell structure. Second, there appears to be a dark dust lane perpendicular to the lobe symmetry axis. The dark waist, or "torus" as it is commonly called, arises naturally due to the density profile of the dust. No torus geometry was explicitly added to the model. The denser regions towards the center of the halo absorb much more of the scattered light than the outer, less dense regions. At some critical distance from the central star, the opacity reaches a point where the light is completely absorbed, naturally creating the appearance of a dust lane. The extent of the bipolarity of the cavity also accentuates this effect. A tighter cavity waist leaves more dust in that region to absorb scattered light and thus the equator becomes dark. Third, we see evidence of a faint glow coming from the tips of the bipolar lobes. As we will see below, this glow turns into directed "searchlight" beams at higher densities. The glow is attributed to light leaking through the cavity walls into the less dense dust halo. Searchlight beams are common among many bipolar nebulae (e.g., the Egg Nebula, Sahai et al. 1998; the Cotton Candy Nebula, Kwok et al. 1998).

3.2. Effects of Dust Density

Figure 3 shows the effects of varying the overall density of the dust halo. The nine panels show the results of increasing the density parameter A. At low densities, the circumstellar dust envelope is optically thin and the equatorial region is bright since the density is higher there and scattered light is stronger. As the

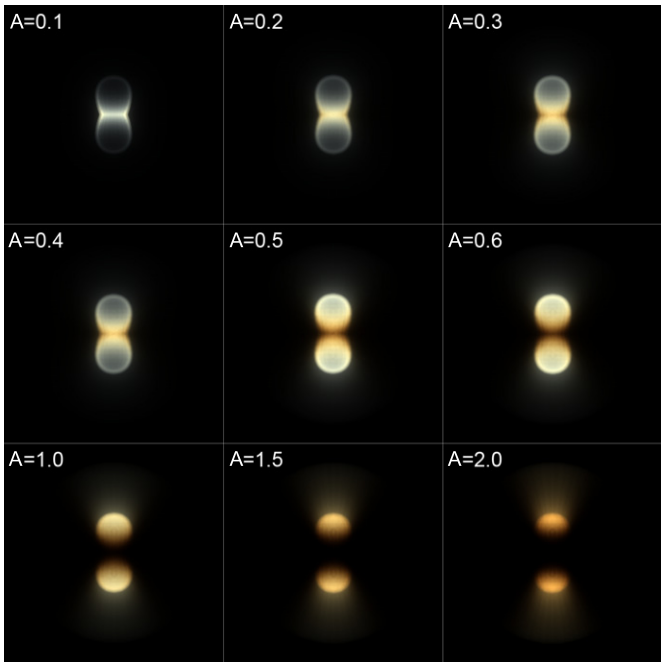

Figure 3. Simulation results for different densities in the dust halo. The images are displayed on a linear intensity scale. The density parameter A is marked on each frame. As the density increases, the dust lane thickens, the searchlight beams become more prominent and the shell morphology gives way to a more volume filled appearance.

(A color version of this figure is available in the online journal.)

dust density increases, a dark lane between the lobes gradually appears. This appearance of this dark lane is the result of the increasing absorption of starlight in the inner region. Contrary to the common assumption that the dark lane corresponds to a torus, our model shows that this is strictly an optical effect and there may not be a separate mass region in the form of a torus. Therefore, an equatorially enhanced outflow during the AGB wind is not necessary, since the bipolar outflow is likely to be collimated at a smaller scale.

One might expect a spherical halo to be visible when the dust is optically thin. The waist of the bipolar lobe is the closest structure to the central star and due to the geometric dilution of light, it is by far the brightest. So although light does leak into the surrounding halo, the overwhelmingly bright bipolar waist hides it if the exposure does not have a sufficiently high dynamic range.

The "glow" seen emanating from the tips of the lobes (as marked on Figure 2) turns into a more directed "searchlight" beam at higher densities (see the bottom row panels of Figure 3). The collimation of the beams is caused by the encroachment of the optically thick region towards the polar region. At lower densities, the waist is relatively thin and light can escape at large angles. At higher densities, however, the thick waist forces the light into the polar regions, thereby producing a more focused feature. The relative brightness of the beams is enhanced when the inner regions are attenuated by the thick waist.

The appearances of the lobes also change with dust density. In the low-density models, the shells of the cavities are more evident, but in the higher density cases, the optical lobes have a more solid appearance.

3.3. Effects of Cavity Size

Figure 4 shows the effect of extending the length of the cavities in the direction parallel to their axis of symmetry. The

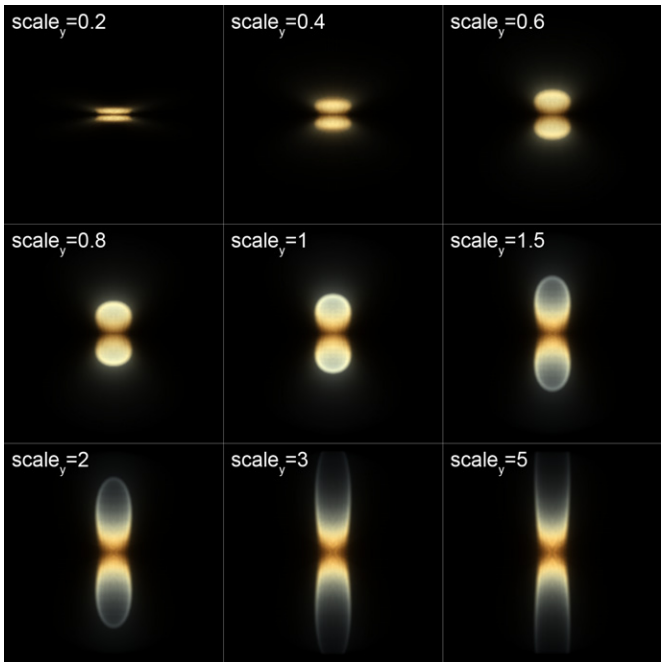

Figure 4. Simulated images as the result of varying sizes of the cavity in one (y) direction. The size scale (ℓ) ranges from 0.2 to 5. A scale of 1 corresponds to a lobe size of 1″. As the scale increases, the cavity displays a more shell-like morphology and the curved bipolar lobes give way to a more cylindrical look.

(A color version of this figure is available in the online journal.)

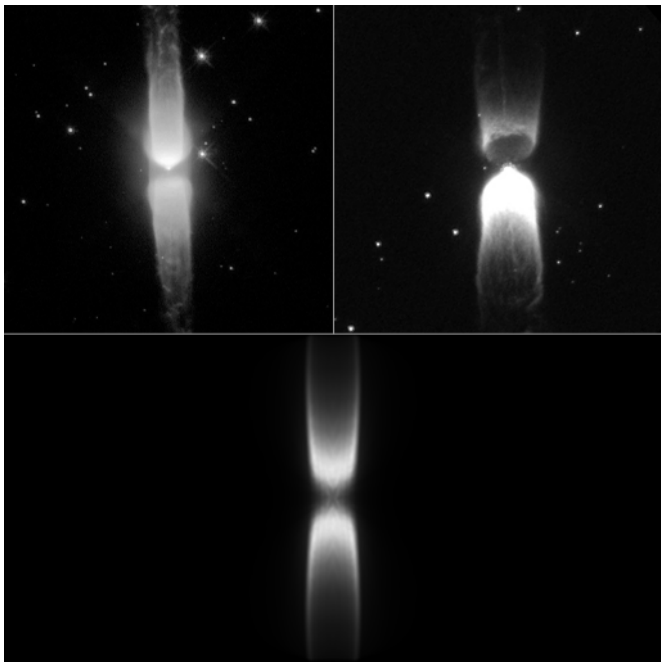

Figure 5. Comparisons between observed reflection nebulae with cylindrical shapes to the model. As the size of the bipolar cavity increases, the curved nature of the lobes disappears and a more cylindrical morphology emerges. Top left: IRAS 10178−5958 (Hen 3-401) (image created from the NASA/ESA/STScI, Hubble Archives, Project GO6816, PI: Sahai). Top right: IRAS 13208−6020 (Image created from NASA/ESA/STScI, Hubble Archives, Project GO10546, PI: Sahai). Bottom: model image with a cavity ℓ factor of 5.

nine panels show the results of increasing the length parameter ℓ from 0.2 to 5. As the bipolar cavities enter the outer regions of the dust halo where the densities are lower, the shell structure of the lobes becomes more evident. The elongated cavities also create a more open-ended cylindrical appearance, similar to the morphology seen in IRAS 10178−5958 (Hen3-401) and IRAS 13208−6020 (Figure 5).

3.4. Effects of Orientation

The effects of orientation on the morphological shapes are illustrated in Figures 6 and 7. For this demonstration, the inclination angle of the cavity with respect to the plane of the sky is rotated between 0° and 90°. Zero degree inclination refers to the edge-on case and at 90° inclination, the bipolar nebulae are viewed pole on. Two sets of cases are shown, corresponding to density parameters of $A = 0.5$ m^{-1} (Figure 6) and $A = 0.1$ m^{-1} (Figure 7).

In the high density (opacity) case, the most evident effect of the rotations is a decrease in brightness of one of the lobes. As one of the lobes is tilted to the front and the other to the back, the back lobes are fainter as the result of dust extinction. Second, at inclinations where the back lobe is still visible, the dust lane appears more three dimensional and begins to resemble a torus. This morphology is seen in several bipolar reflection nebulae such as IRAS 16243−3814, IRAS 19292+1806, and IRAS 19343+2926 (Minkowski's Footprint) (Figure 8). At inclinations approaching 90°, we can no longer see the back lobe but an inner "ring" appears, which is actually the part of the lobes closest to the central star. Although PPNs seen at this orientation are overwhelmed by the light of the star (these simulations do not render the light from the star), some ring structures have been observed in PPNs (e.g., IRAS 20462+3416 and IRAS 11385−5517) and are commonly seen in young

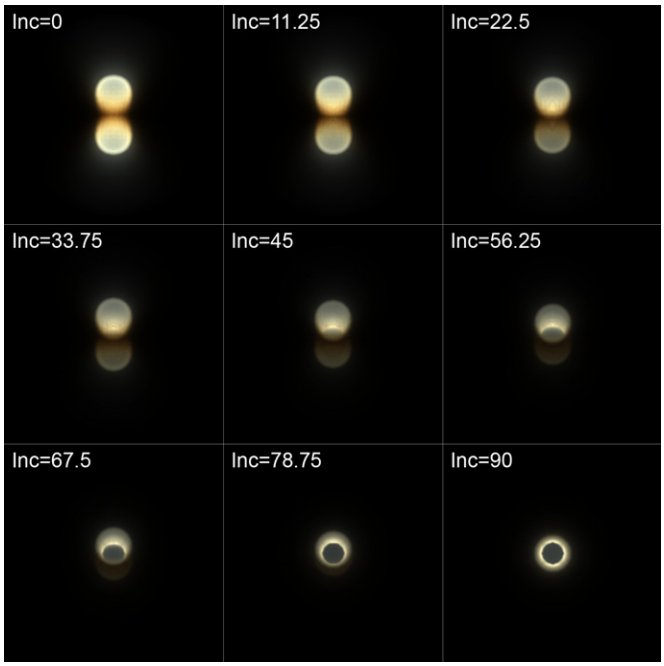

Figure 6. Simulated images as viewed from different directions. The inclination angle is marked on each frame. The model is for the case $A = 0.5$ m^{-1}. As the inclination increases, the back lobe becomes fainter and the dust lane takes on a torus appearance.

(A color version of this figure is available in the online journal.)

planetary nebulae where the nebula is much brighter as in IRAS 15318−7144 (Hen2-131) (Figure 9).

In the low opacity case, the back lobe still gets dimmer, but is clearly visible at all inclinations. As the inclination increases,

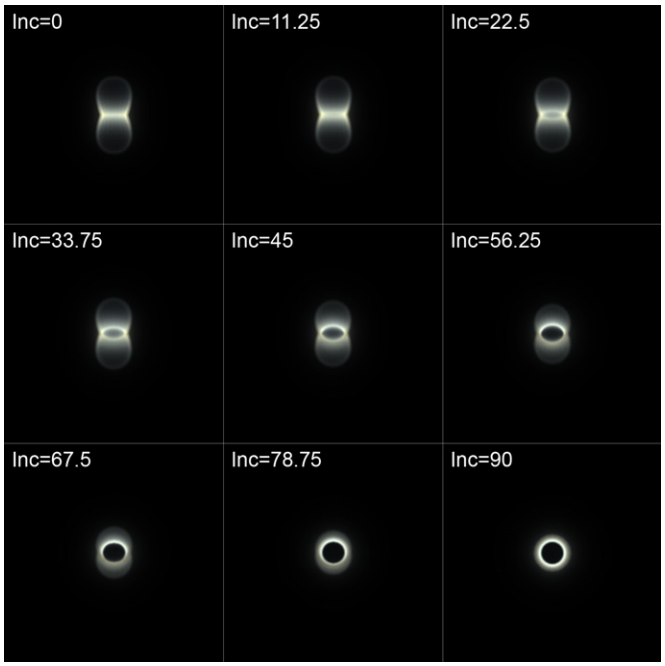

Figure 7. Simulated images as viewed from different directions for the low-density ($A = 0.1$ m^{-1}) case. The inclination angle of each simulation is indicated in the image panels. As the inclination increases, a ring like structure appears in the center surrounded by a faint elliptical structure.

(A color version of this figure is available in the online journal.)

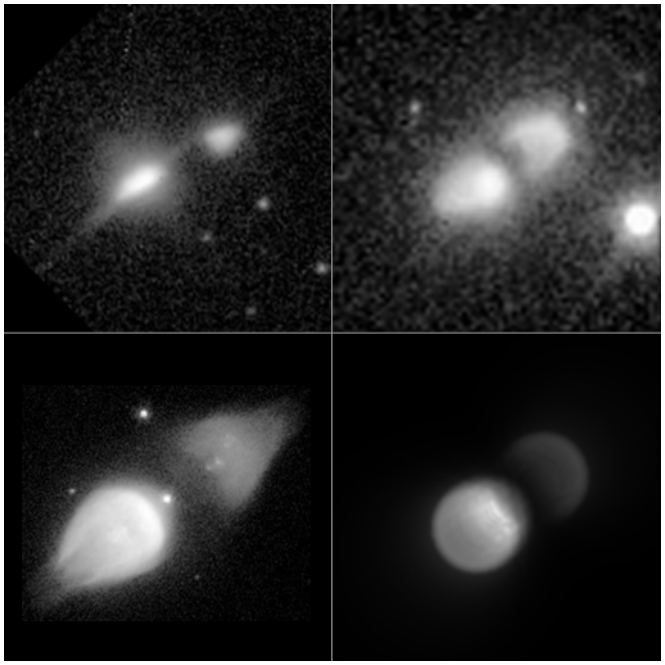

Figure 8. Many bipolar reflection nebulae show a well-defined, thick "torus" around their waist. This morphology is well reproduced by the model at a non-zero inclination angle. From left to right, top to bottom: IRAS 16243−3814 (image created from NASA/ESA/STScI, Hubble Archives, Project GO6364, PI: Bobrowsky); IRAS 19292+1806 (image created from NASA/ESA/STScI, Hubble Archives, Project GO9463, PI: Sahai); IRAS 19343+2926 (image created from NASA/ESA/STScI, Hubble Archives, Project GO6533, PI: Buharrabal); model image for the density parameter $A = 0.5$ m^{-1} with an inclination of 45°.

a bright central ring appears (the inner regions of the lobes), surrounded by a faint elliptical lobe that appears extended around the inner ring. This morphology has been observed in PPNs such as IRAS 17436+5003 and IRAS 02229+6208.

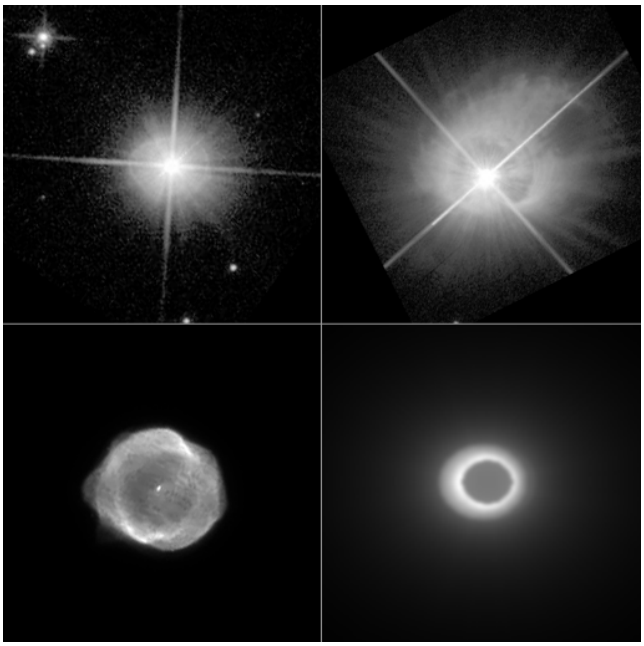

Figure 9. When viewed pole on, the model (bottom right) appears ring-like surrounded by a faint outer halo. This morphology is similar to some PPNs (top images) and many young PNs (bottom left image). Left to right, top to bottom: IRAS 20462+3416 (image created from NASA/ESA/STScI, Hubble Archives, Project GO6364, PI: Bobrowsky); IRAS 11385−5517 (image created from NASA/ESA/STScI, Hubble Archives, Project GO69463, PI: Sahai); IRAS 15318−7144 (Young PN; image created from NASA/ESA/STScI, Hubble Archives, Project GO6119/6353, PI: Bond/Sahai); model image at an inclination of 90° and $A = 0.5$ m^{-1}. Direct light from the central star is not rendered in the model image.

3.5. Effects of Non-evacuated Cavity

It may be possible that the dust within the evacuated cavity is not completely removed, and a small fraction remains through entrainment of the largest grains. This section investigates the morphological consequences of the small amounts of dust remaining in the cavity. The results are presented in Figure 10 where the density of the cavity (n_c) is varied from $f = 0$ to $f = 0.01$, where $n_c = f \times n_0$.

The only noticeable effect of a non-evacuated cavity is the bright region that appears at the center of the nebula. This feature is not the star (which is not rendered in these simulations), but light being scattered by the little dust that remains. Due to the density profile of the halo, this remaining dust is concentrated near the center, giving a "star-like" appearance. Compounding this effect is the fact that due to geometric dilution, the dust closest to the star will receive much more light than that further away. It is interesting to note how little dust is required in the cavity to create this effect (the "star" is visible even when the dust is 99.9% evacuated). This suggests that the colors that one observes for the central "star" may not represent the actual color of the central star, but only reflect the colors of the central dust region.

These bright regions are seen within the dark equatorial waist of many bipolar nebulae (Figure 11) and are assumed to be the actual central star. In light of this simulation, however, this central region may instead be light reflecting off small traces of dust or a combination of both.

3.6. Evolutionary Sequence

These models can be applied to the evolution of PPNs. This transition stage is defined by an absence of photo-ionizing

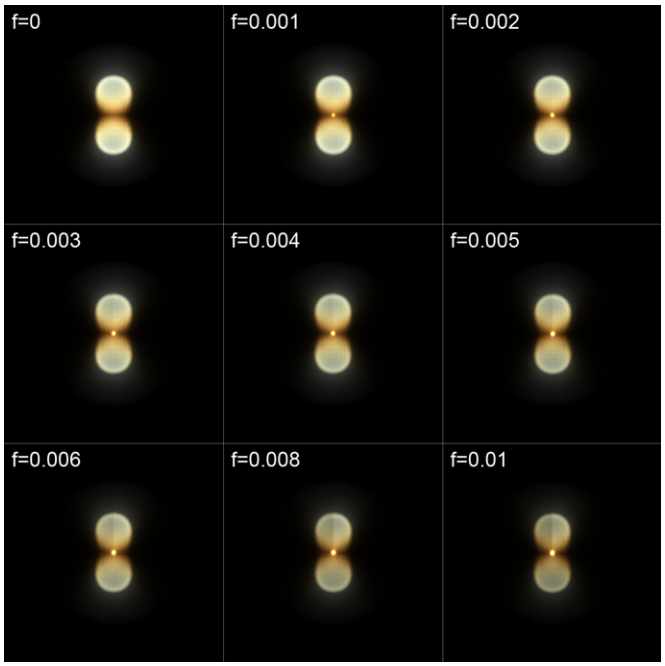

Figure 10. Simulated images showing the effect of having small traces of dust remaining in the cavity. The cavity density is given by $n_c(r) = f n_0(r)$, where $n_0(r)$ is the dust density in the envelope at distance r from the central star. The brightness scale for all images has been normalized to the first image at $f = 0$.

(A color version of this figure is available in the online journal.)

Figure 11. Example of several bipolar reflection nebulae and proto-planetary nebulae that display a bright central "star-like" region. From left to right, top to bottom: M1−92 (image created from NASA/ESA/STScI, Hubble Archives, Project GO6533, PI: Buharrabal); IRAS 13208−6020 (image created from NASA/ESA/STScI, Hubble Archives, Project GO10536, PI: Sahai); IRAS 20068+4051 (image created from NASA/ESA/STScI, Hubble Archives, Project GO10536, PI: Sahai), IRAS 17150−3224 (image created from NASA/ESA/STScI, Hubble Archives, Project GO6565, PI: Kwok).

radiation from the central star and the optically bright nebulosity is strictly due to the result of dust scattering. The dynamical evolution of a PPN can be modeled by the expansion of the halo and the initiation of a fast outflow that evacuates part of the AGB envelope. As the PPN evolves, the density of the dust

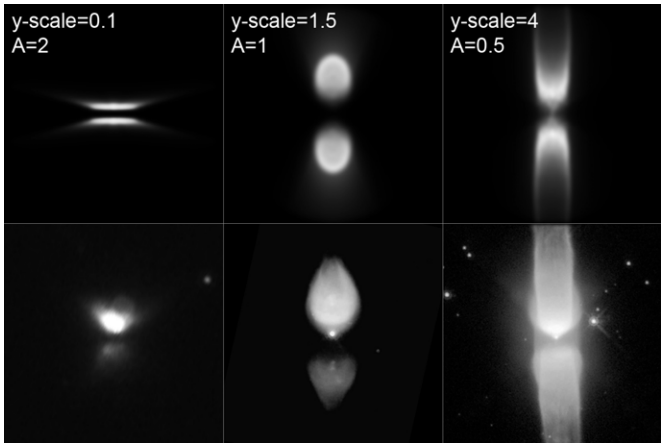

Figure 12. Top row: a simulation of evolutionary progression in morphology as the lobes get larger and the density of the dust halo drops. Evolution in age is from left to right. The model parameters are given in each of the three panels. A Gaussian convolution was applied to simulate the diffraction pattern of the telescope. Bottom row: observed images selected as examples of possible observational counterparts of the simulated images. From left to right: IRAS 13557−6442 (image created from NASA/ESA/STScI, Hubble Archives, Project GO9463, PI: Sahai); IRAS 19343+2926 (image created from NASA/ESA/STScI, Hubble Archives, Project GO6533, PI: Buharrabal); IRAS 10178−5958 (image created from NASA/ESA/STScI, Hubble Archives, Project GO6816, PI: Sahai).

halo will drop as the dust spreads spherically throughout space. If the evacuating mechanism is no longer active, then the cavity will still continue to grow as the dust evolves. If the mechanism remains active for a lengthly period of time, then the cavity may reach the outside of the dust halo and break through the outer boundary.

What are the morphological implications of this dynamical evolution? As we have seen, a decrease in dust density directly impacts the size of the dark equatorial waist. A lower density implies a tighter waist. Additionally, when the density is low, the "searchlight" beams turn into a diffuse glow. The once optically thick cavity walls become transparent to light, and thus a more shell like instead of volume filled structure is observed.

As the cavity grows in size along the symmetry axis, we have seen that the bipolar curve tends to flatten out, giving a more linear appearance to the lobes (Figure 4). Furthermore, as the cavity extends into the less dense outer regions of the dust halo, the opacity in the shell becomes lower and thus we see more of a shell like structure. If the cavity grows beyond the dust halo, then the bipolar lobes no longer connect and the nebula appears cylindrical.

These simulations therefore hint at a possible morphological evolutionary sequence of a PPN. At an early stage of the post-AGB phase, the density of the circumstellar dust envelope is relatively large and the size of the lobes relatively small. Thus, the PPN will have a thick dust lane with respect to the lobes which may appear volume filled. This young PPN may also exhibit searchlight beams, as the thick disk will channel the light through the polar regions. As the PPN evolves, the dust lane will get thinner as the lobes get larger and straighten out. The lobes will gradually appear more shell like in structure and eventually cylindrical as the cavity pierces the outer boundary of the dust halo. Figure 12 shows this evolutionary sequence with possible observational counterparts shown in the lower panels.

The panels of Figure 12 (from left to right) decrease in density (A value) by a factor of two for each successive panel. If we assume a constant expansion velocity of $\sim v = 10\,\mathrm{km\,s^{-1}}$ and

an initial radius of 4.5×10^{11} km (3″ halo radius at 1 kpc), then we can make an estimate as to the evolutionary time-scale. A density drop of 0.5 requires a two-fold increase in volume:

$$V_2 = 2V_1 = 2\frac{4}{3}\pi r_1^3 = \frac{4}{3}\pi(r_1 + vt)^3, \quad (1)$$

where V_1 and r_1 are the volume and radius of the halo in the first panel, respectively, and V_2 is the volume in the second panel. Solving Equation (1) for time gives

$$t \sim 0.25\frac{r_1}{v}. \quad (2)$$

Using our values, we find that the time taken to go from panel 1 to panel 2 in Figure 12 is ∼356 years. Similarly, to go from panel 2 to panel 3 (another drop in density by a factor of 2) is ∼445 years. Therefore, the time taken for the PPN morphology to evolve (given our initial conditions) is ∼800 years.

Of course, the initial density of the dust halo at the onset of the PPN phase will vary from object to object. Thus, we must be careful when applying this morphological evolution to determine the relative age of PPNs. For example, if the AGB star shed little dust, then the density would be initially low, giving a thin dust lane from the beginning. Similarly, if the dust halo is very large and dense, then an older PPN may still show very round bipolar lobes where a younger PPN in a small, sparse dust halo will show cylindrical lobes.

4. DISCUSSION

Many bipolar PPNs show evidence of a dark equatorial region, commonly attributed to high density dust in the form of a torus. The origin of this dense equatorial region, however, has never been satisfactorily explained. Several mechanisms that employ both single and binary stars have been suggested. Many single star models require the fast rotation of the AGB star (Asida & Tuchman 1995) to account for the preferred equatorial flow either through centrifugal or magnetic forces(Matt et al. 2000). The Wind Compressed Disk (WCD) model proposed by Bjorkman & Cassinelli (1993) provides a mechanism for which the winds can be focused towards the equator and is one of the most promising single star models (see discussion in Balick & Frank 2002). Finally, binary models have been considered in which Roche lobe overflow or Bondi accretion of AGB winds can lead to accretion disks (e.g., Mastrodemos & Morris 1998) and the necessary equatorial density enhancement (Mastrodemos & Morris 1999).

Here, we suggest that the optically bright bipolar lobes do not represent regions of high density, but rather a low-density region illuminated by a central star. The density profile of the halo, combined with a bipolar cavity, naturally produces this observed structure. The cavity, presumably, was created by a fast, collimated ejection that swept clean the circumstellar material. The novelty of this hypothesis, however, is that the torus need not be a separate structure with a distinct boundary. The torus and the bipolar lobes do not represent two separate ejection events (see, e.g., Huggins 2007), but are different manifestations of a single physical event. This has implications for the formation mechanism behind PPNs, since whatever mechanism is responsible for the formation of the cavity is automatically responsible for the formation of the torus. This explanation therefore greatly simplifies the theoretical model required to explain the observations.

We note that in this model we have not addressed the physical origin of the cavities. We have just assumed that the cavities are created as a result of a collimated fast outflow from the central star sweeping clean the circumstellar envelope in specific directions. This outflow needs not be massive, as only high momentum/energy of the outflow (as the result of high wind velocity) is adequate in achieving this effect. Depending on whether the interaction between the fast outflow and the circumstellar envelope is isothermal or adiabatic, the mass loss rate of the fast outflow can be several orders of magnitude smaller than the mass loss rate that created the pre-existing circumstellar envelope.

We find that small traces of dust remaining in the cavity can give rise to a bright, star-like region at the center of the nebula. The profile on the density of the halo and the geometric dilution of light combines to accentuate this effect. There are implications if this bright region is indeed caused by scattered light from dust and not the central star. First, this gives us some insight into the mechanism that created the cavity. For example, if the evacuating mechanism is a jet, then it must not be too dense. Second, there may be implications for the derived properties of the central star, such as the temperature from SEDs, since scattered light will appear bluer. Distinguishing between the two scenarios and understanding the implications require further study.

The hypothesis prompting this study, namely that lobes appearing volume filled may in fact be empty cavities, is strongly supported by the results of this analysis. Our simulations show that if the density of the dust halo is high enough, then the opacity becomes such that the cavities will appear volume filled. When the density is low, the lobes show their true shell-like structure. The volume filled appearance is strongly dependant on the opacity created by the cavity shell, which in turn is dependant on properties such as thickness and density These properties may shed light onto the mechanism that evacuated the cavities and swept up the shell material. For example, it can be shown using shock physics (see, for example, Kwok 2007) that the density and width of the shell are related to the speed of the shock and therefore the speed and density of the jet. Although the exact mechanism responsible for creating the cavities is unknown at this time, it must involve a fast, at least partially collimated, wind of low density. The speed of the wind must be high enough to sweep up and compress the circumstellar material, and the density must be low enough not to fill up the cavity with new material. The interaction can be adiabatic or isothermal, depending on how effectively the swept-up materials are cooled. Additionally, the evacuating mechanism must not destroy all of the dust, but instead sweep it up. This places additional constraints on the shock speed. Hydrodynamic simulations by Van Marle et al. (2011) suggest that small grains will form a shell preferentially to larger grains in an interaction between a wind and the ISM. The size of the shell may therefore have implications on the grain size and composition of the dust.

Although this paper focuses on post-AGB objects, the mechanism discussed is also applicable to other classes of bipolar reflection nebulae. For example, Gomez's Hamburger (Ruiz et al. 1987) and the Homunculus nebula around Eta Carinae are examples of non-post-AGB bipolar reflection nebulae, whose morphologies are likely influenced by selective illumination.

5. CONCLUSIONS

We have shown that many of the observed morphological features of bipolar reflection nebulae can be reproduced by a

simple model consisting of a bipolar cavity embedded in a dense dust halo. First, the thick equatorial "torus" seen in the waist of bipolar nebulae could be nothing more than a consequence of the cavity within a dust halo. Second, the filled appearance of the lobes does not represent a volume of material, but simply optically thick cavity walls. Third, the bright central region may be due to light scattered off of remnant dust instead of the star itself.

Our results show that illumination effects play an important role in defining the optical morphology of bipolar reflection nebulae. Before one rushes into physical mechanisms to model the nebular structure, one has to first carefully consider these effects and their implications.

N.K. acknowledges support from the Natural Sciences and Engineering Research Council of Canada (NSERC), the Alberta Ingenuity Fund and the Killam Trusts. This work was supported by a grant to S.K. from the Research Grants Council of the Hong Kong Special Administrative Region, China (Project No. HKU 7031/10P). W.S. acknowledges support by grants from CONACYT 49447 and UNAM PAPIIT IN100410, as well as from the Alexander von Humboldt Foundation.

REFERENCES

Alcolea, J., Neri, R., & Bujarrabal, V. 2007, A&A, 468, L41
Asida, S. M., & Tuchman, Y. 1995, ApJ, 455, 286
Balick, B., & Frank, A. 2002, ARA&A, 40, 439
Bjorkman, J. E., & Cassinelli, J. P. 1993, ApJ, 409, 429
Bujarrabal, V., Alcolea, J., Sahai, R., Zamorano, J., & Zijlstra, A. A. 1998, A&A, 331, 361
Bujarrabal, V., Alcolea, J., Soria-Ruiz, R., et al. 2010, A&A, 521, L3
De Marco, O., Bond, H., Harmer, D., & Fleming, A. 2004, ApJL, 602, L93
García-Lario, P., Riera, A., & Manchado, A. 1999, ApJ, 526, 854
García-Segura, G., Langer, N., Rozyczka, M., & Franco, J. 1999, ApJ, 517, 767
Hrivnak, B. J., Smith, N., Su, K. Y. L., & Sahai, R. 2008, ApJ, 688, 327
Huggins, P. J. 2007, ApJ, 663, 342
Kwok, S. 1995, ARA&A, 31, 63
Kwok, S. 2001, Origin and Evolution of Planetary Nebulae (Cambridge: Cambridge Univ. Press)
Kwok, S. 2004, in ASP Conf. Ser. 313, Asymmetric Planetary Nebulae III, ed. M. Meixner et al. (San Francisco, CA: ASP), 580
Kwok, S. 2007, Physics and Chemistry of the Interstellar Medium (Sausalito, CA: Univ. Science Books)
Kwok, S. 2010, PASA, 27, 174
Kwok, S., Hrivnak, B. J., & Su, K. Y. L. 2000, ApJL, 544, L149
Kwok, S., Su, K. Y. L., & Hrivnak, B. J. 1998, ApJL, 501, L117
Lagadec, E., Verhoelst, T., Mékarnia, D., et al. 2011, MNRAS, 417, 32
Mastrodemos, N., & Morris, M. 1998, ApJ, 497, 303
Mastrodemos, N., & Morris, M. 1999, ApJ, 523, 357
Mathis, J. S., Rumpl, W., & Nordsieck, K. H. 1977, ApJ, 217, 425
Matt, S., Balick, B., Winglee, R., & Goodson, A. 2000, ApJ, 545, 965
Muthumariappan, C., Kwok, S., & Volk, K. 2006, ApJ, 640, 353
Ruiz, M. T., Blanco, V., Maza, J., et al. 1987, ApJL, 316, L21
Sánchez-Contreras, C., Sahai, R., & Gil de Paz, A. 2002, ApJ, 578, 269
Sahai, R., Hines, D. C., Kastner, J. H., et al. 1998, ApJL, 492, L163
Sahai, R., Morris, M., Sanchez Contreras, C., & Claussen, M. 2007, AJ, 134, 2200
Sahai, R., & Nyman, L.-Å 1997, ApJL, 487, L155
Steffen, W., Koning, N., Wenger, S., Morisset, C., & Magnor, M. 2011, IEEE Trans. Vis. Comput. Graphics, 17, 454
Su, K. Y. L., Kelly, D. M., Latter, W. B., et al. 2004, ApJS, 154, 302
Van Marle, A. J., Meliani, Z., Keppens, R., & Decin, L. 2011, ApJL, 734, L26